

NUMERICAL CALCULATION OF CONFINED COAXIAL TURBULENT SWIRLING JETS

Yong Gang Xu
 XI'AN aero-engine (group) Ltd.

Keywords: *non-orthogonal, transformation, turbulent, swirling, jet*

Abstract

In this paper, a non-orthogonal coordinate transformation method presented in reference [1] has been used to develop a computation method for the prediction of confined coaxial turbulent swirling jets with imposed adverse pressure gradient. A computer code has been developed. In the program, the standard $k-\epsilon$ model has been used. For the finite-difference approximation to the convection terms, a combination of the HYBRID scheme and the second-order upwind scheme has been used. For the swirling conditions, a modified $k-\epsilon$ model has been adopted. Then, the program has been applied to predictions of the experimental condition under which non-swirling flow with imposed adverse pressure gradient has been observed [2]. The comparison of the computation results with the experimental results shows rather fine agreement. Later, numerical predictions have been made for a case of contra-swirling turbulent jet with imposed adverse pressure gradient, and a case of contra-swirling turbulent jet with sudden expanding confinement. It is observed that for fixed grids, numerical predictions are influenced considerably by the inlet turbulent conditions. Therefore, inlet turbulent quantities must be specified realistically if quantitatively correct results are desired.

1 Introduction

In the design process of a combustion chamber, there are many ingredients involved. It is hardly possible for effects of these ingredients to be expressed by a simple experiential equation. In general, the design is largely

dependent on various experiments. It is self-evident that numerical prediction by establishing calculating models of combustion chambers has obvious advantage over pure experiments. For many years, researching workers have done jobs with confined jets on the inert condition and the exothermic condition. Now that most of the real configurations of combustion chambers are of varying sections, on these conditions (with imposed adverse pressure gradient), investigating to predict the field development of coaxial confined jets using numerical calculation, so as to grasp the loss rule of the airflow will be undoubtedly of great importance for the improvement of the chamber design and the combustion efficiency.

Because of the abnormality of the problem domain being investigated, there rises difficulty in the numerical solution. In order to solve this problem, J. F. Thompson ([3], [4]) etc. applies the boundary-fitted transformation to computational fluid dynamics, so as to make the boundary conditions easier to be treated and promote the calculating precision.

The primary aspect of the boundary-fitted coordinate system is how to form the grids. And the differences in mesh producing will directly affect the complexity of the controlling equations and the calculating. In 1984, the methodology of forming grids with algebraic non-orthogonal coordinate transformation was put forward in reference [1]. The main merit of this method is to avoid the numerical solution of elliptic equations, and the controlling equations are also straightforward.

In point of engineering numerical calculation, the most frequently used turbulent solving method is the Reynolds time-average method.

When the time-average method is used, the pulsant correlation terms will exist, so it is necessary to establish a turbulent model. There are a wide variety of turbulent models. The variety adopted in this paper is based on the concept of vortex viscosity presented in 1877 by Boussinesq, that is

$$-\overline{u_i' u_j'} = \nu_t (u_{,j} + u_{,i}) - \frac{2}{3} \delta_{ij} K$$

Therefore, the primary task of this model is to put forth an estimation method of the vortex viscosity coefficient ν_t . According to the number of partial differential equations included in the extra relations introduced during the estimation of vortex viscosity coefficient, there will be the null-equation model, the one-equation model and the two-equation model, and so on. In consideration of the universality of the current engineering use and the convenience of computation, it is feasible to adopt the $k-\varepsilon$ two-equation model.

In this paper, on the basis of the former work of others, by using the thought of non-orthogonal transformation in the Cartesian coordinate system put forth in reference [1], combined with the turbulent flow controlling equations in the cylindrical coordinate system and the $k-\varepsilon$ two-equation model, a computation methodology of coaxial confined turbulent swirling jets has been developed, which could be used either to constant-section case or to variable-section case. Compared with [1], apart from the difference of the coordinate system, the other characteristic of this paper is that the velocity component solved on the computational plane is the very velocity on the physical plane, which is more obvious and more convenient. Because on the swirling condition, the hypothesis of vortex viscosity – isotropy is not satisfied, a bad accuracy is gained if one uses the standard $k-\varepsilon$ model. Therefore, on the swirling (co-swirling or contra-swirling) condition, this paper adopts the modified $k-\varepsilon$ model constants presented in reference [5]. In the non-swirling case, however, the standard $k-\varepsilon$ model constants are still used. By applying the procedure of this paper to the experimental data presented in reference [2] for a non-swirling

coaxial confined jet with imposed adverse pressure gradient, a numerical prediction has been made. The comparison of the computation results with the experimental results shows rather fine agreement.

2 Theoretic Analysis and Numerical Calculation

2.1 Controlling Equations on the Physical Plane

In the axisymmetrical case, the physical plane is the r - z plane (meridian plane), as shown in Fig. 2.1. The basic controlling equations in the cylindrical coordinate system are as follows.

1) The continuity equation

$$\frac{\partial(\rho u)}{\partial z} + \frac{1}{r} \frac{\partial}{\partial r} (\rho r v) = 0$$

2) The momentum equations

A. Radial (r direction)

$$\frac{\partial}{\partial z} (\rho u v) + \frac{1}{r} \frac{\partial}{\partial r} (\rho r v v) = \frac{\partial}{\partial z} (\mu_{eff} \frac{\partial v}{\partial z}) + \frac{1}{r} \frac{\partial}{\partial r} (\mu_{eff} r \frac{\partial v}{\partial r}) + S^v$$

$$\text{where } S^v = \frac{\partial}{\partial z} (\mu_{eff} \frac{\partial u}{\partial r}) + \frac{1}{r} \frac{\partial}{\partial r} (r \mu_{eff} \frac{\partial v}{\partial r}) - \frac{\partial p}{\partial r} - 2\mu_{eff} \frac{v}{r^2} + \frac{\rho w^2}{r}$$

B. Axial (z direction)

$$\frac{\partial}{\partial z} (\rho u u) + \frac{1}{r} \frac{\partial}{\partial r} (\rho r v u) = \frac{\partial}{\partial z} (\mu_{eff} \frac{\partial u}{\partial z}) + \frac{1}{r} \frac{\partial}{\partial r} (\mu_{eff} r \frac{\partial u}{\partial r}) + S^u$$

$$\text{where } S^u = \frac{\partial}{\partial z} (\mu_{eff} \frac{\partial u}{\partial z}) + \frac{1}{r} \frac{\partial}{\partial r} (r \mu_{eff} \frac{\partial v}{\partial z}) - \frac{\partial p}{\partial r}$$

C. Circumferential (θ direction)

$$\frac{\partial}{\partial z} (\rho u w) + \frac{1}{r} \frac{\partial}{\partial r} (\rho r v w) = \frac{\partial}{\partial z} (\mu_{eff} \frac{\partial w}{\partial z}) + \frac{1}{r} \frac{\partial}{\partial r} (\mu_{eff} r \frac{\partial w}{\partial r}) + S^w$$

$$\text{where } S^w = -\frac{\rho v w}{r} + \frac{1}{r} (\mu_{eff} \frac{\partial w}{\partial r}) - \frac{\partial}{\partial r} (\mu_{eff} \frac{w}{r}) - \frac{2}{r} (\mu_{eff} \frac{w}{r})$$

3) k equation

$$\frac{\partial}{\partial z} (\rho u k) + \frac{1}{r} \frac{\partial}{\partial r} (\rho r v k) = \frac{\partial}{\partial z} \left(\frac{\mu_{eff}}{\sigma_k} \frac{\partial k}{\partial z} \right) + \frac{1}{r} \frac{\partial}{\partial r} \left(\frac{\mu_{eff}}{\sigma_k} r \frac{\partial k}{\partial r} \right) + S^k$$

where $S^k = G - \rho \varepsilon$

4) ε equation

$$\frac{\partial}{\partial z} (\rho u \varepsilon) + \frac{1}{r} \frac{\partial}{\partial r} (\rho r v \varepsilon) = \frac{\partial}{\partial z} \left(\frac{\mu_{eff}}{\sigma_\varepsilon} \frac{\partial \varepsilon}{\partial z} \right) + \frac{1}{r} \frac{\partial}{\partial r} \left(\frac{\mu_{eff}}{\sigma_\varepsilon} r \frac{\partial \varepsilon}{\partial r} \right) + S^\varepsilon$$

where $S^\varepsilon = \frac{\varepsilon}{k} (C_1 G - C_2 \rho \varepsilon)$

In 3) and 4), G is the generated term:

$$G = \mu_{eff} \left\{ 2 \left[\left(\frac{\partial u}{\partial z} \right)^2 + \left(\frac{\partial v}{\partial r} \right)^2 + \left(\frac{v}{r} \right)^2 \right] + \left(\frac{\partial u}{\partial r} + \frac{\partial v}{\partial z} \right)^2 + \left[\left(\frac{\partial w}{\partial z} \right)^2 + \left(\frac{\partial w}{\partial r} - \frac{w}{r} \right)^2 \right] \right\}$$

The term μ_{eff} in 2), 3) and 4) is the effective viscosity:

$$\mu_{eff} = \mu + \mu_t, \quad \mu_t = C_\mu \rho \frac{k^2}{\varepsilon}$$

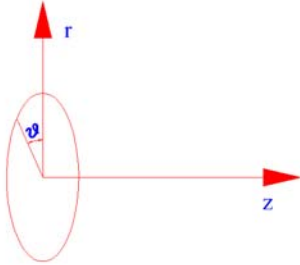


Fig. 2.1

Constants in table 2.1 are the standard $k-\varepsilon$ model constants, for the swirling jet conditions, the study in reference [5] proved that a more realistic flow field profile could be attained if the modified $k-\varepsilon$ model constants shown in table 2.2 were adopted.

Table 2.1 The Standard $k-\varepsilon$ Model Constants

C_μ	C_1	C_2	σ_k	σ_ε
0.09	1.44	1.92	1.00	1.30

Table 2.2 The Modified $k-\varepsilon$ Model Constants for Swirling Flow

C_μ	C_1	C_2	σ_k	σ_ε
0.125	1.44	1.5942	1.00	1.1949

The above basic controlling equations can take the following more general form:

$$\frac{\partial}{\partial z} (\rho u \Phi) + \frac{1}{r} \frac{\partial}{\partial r} (\rho r v \Phi) = \frac{\partial}{\partial z} \left(\Gamma_\Phi \frac{\partial \Phi}{\partial z} \right) + \frac{1}{r} \frac{\partial}{\partial r} \left(\Gamma_\Phi r \frac{\partial \Phi}{\partial r} \right) + S^\Phi \quad (A)$$

When Φ takes $l, v, u, w, k, \varepsilon, \Gamma_\Phi$ takes $\theta, \mu_{eff}, \mu_{eff}$.

$\mu_{eff}, \frac{\mu_{eff}}{\sigma_k}, \frac{\mu_{eff}}{\sigma_\varepsilon}$, and S^Φ takes $\theta, S^v, S^u, S^w, S^k, S^\varepsilon$,

we can get the continuity equation, the radial momentum equation (v equation), the axial momentum equation (u equation), the circumferential momentum equation (w equation), the k equation and the ε equation.

2.2 Controlling Equations on the Computational Plane

For the irregular domain in the Cartesian coordinate system where one wall lies along the axis, it was put forth in reference [1] that using algebraic non-orthogonal coordinate transformation:

$$\xi = \frac{x}{w(y)}, \quad \eta = y,$$

we could transform the flow field from an irregular domain on the physical plane into a regular domain on the computational plane: the boundaries of the computational domain coincide with the ξ and η axes, as shown in Fig. 2.2.

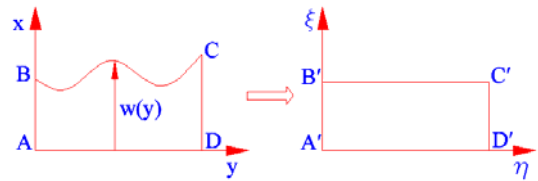


Fig. 2.2

Because the transform is algebraic, no elliptic equation about body-fitted coordinates is added, and the computation is reduced remarkably. At the same time, as no numerical approximation element has been introduced into the transform plane equations and the body-fitted coordinates, the body-fitted effects can be eliminated completely, and the transform plane

equations can be coupled completely with the original physical problems.

In this paper, making use of that transformation thought, the following transforms are introduced:

$$\xi = \xi(r, z) = \frac{r}{w_r(z)}, \quad \eta = \eta(r, z) = z$$

to transform the flow field from an irregular domain on the r - z physical plane into a regular domain on the ξ - η computational plane, with the boundaries of the computation domain coinciding with the ξ and η axes, as shown in Fig. 2.3. In the mean time, the equations on the physical plane will change into the equations on the computational plane.

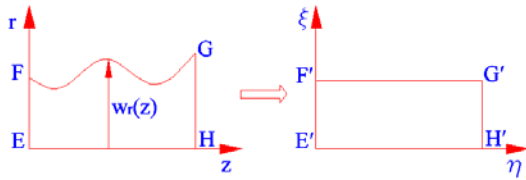


Fig. 2.3

After transformation, the universal variable form of the controlling differential equations on the computational plane is as follows.

$$\frac{\partial J_\eta}{\partial \eta} + \frac{\partial J_\xi}{\partial \xi} = J \zeta S^{\Phi'}(\zeta, \eta) - \frac{\partial}{\partial \eta} \left(\frac{\Gamma_\Phi \xi}{J} q_2 \Phi_\eta \right) - \frac{\partial}{\partial \xi} \left(\frac{\Gamma_\Phi \xi}{J} q_2 \Phi_\eta \right) \quad (B)$$

where

$$J = \begin{vmatrix} r_\xi & z_\xi \\ r_\eta & z_\eta \end{vmatrix}$$

$$J_\eta = \rho \bar{u} \Phi - \frac{\Gamma_\Phi \xi}{J} q_3 \Phi_\eta, \quad J_\xi = \rho \bar{v} \Phi - \frac{\Gamma_\Phi \xi}{J} q_1 \Phi_\xi$$

$$q_1 = r_\eta^2 + z_\eta^2, \quad q_2 = r_\xi r_\eta + z_\xi z_\eta, \quad q_3 = r_\xi^2 + z_\xi^2$$

$$S^{\Phi'}(\zeta, \eta) = -\frac{\rho u \Phi r_\eta}{J \xi} + \frac{\Gamma_\Phi}{J^2 \xi} (r_\xi \Phi_\eta - r_\eta \Phi_\xi) + S^\Phi(\zeta, \eta)$$

$$\bar{u} = ur_\xi - vz_\xi, \quad \bar{v} = vz_\eta - ur_\eta$$

\bar{u} (\bar{v}) is the velocity in the η (ξ) direction on the computational plane.

For the continuity equation, the universal variable form is:

$$\frac{\partial J_\eta}{\partial \eta} + \frac{\partial J_\xi}{\partial \xi} = J \zeta S^{\Phi'}(\zeta, \eta)$$

$$\text{where } S^{\Phi'}(\zeta, \eta) = -\frac{\rho u r_\eta}{J \xi}$$

Refer to the appendix for the specific Γ_Φ and $S^{\Phi'}$ expressions of the remaining equations.

2.3 The domain discretization and the finite-difference forms of the controlling equations

In order to deduce the finite-difference forms of the controlling equations, this paper adopts the finite-volume method: at first, divide the calculation domain into many control volumes which do not overlap each other, and make each grid point surrounded by a control volume. Then integrate the differential equations over each control volume, calculate the required integral using the subsection-distributing relation expressing the Φ variation between grid points. The advantage of using the finite-volume method is that the attained results of the mass, the momentums and other variables will precisely meet the integral conservation over any set of control volumes, and naturally over the entire calculating domain. For any number of grid points, this character will exist, and the precise integral balance could be attained even for the solution of coarse grids.

If during the discretization, we integrate the quantities such as velocities, pressure, turbulent kinetic energy and its diffusive rate over the same set of grids, the velocity field and the pressure field of numerical solution may be unrealistic and fluctuant [6]. The appropriate way to solve this problem is adopting staggered grids, to solve velocity u , velocity v and pressure p etc over three different sets of grids, as shown in Fig. 2.4.

Integrating differential equation (B) over a control volume – typically the main control volume (control volume of pressure p , turbulent kinetic energy k , diffusive rate ε and circumferential velocity w) enclosing grid point P in Fig. 2.4, with the control volume $d\bar{V} = \zeta_p d\eta d\xi$, we get

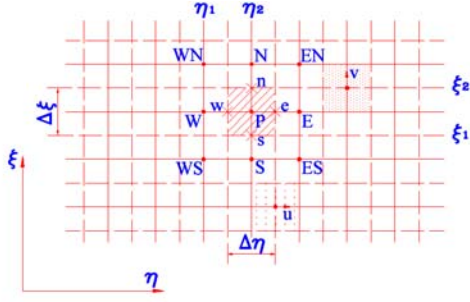


Fig. 2.4

$$\iint_{c,v} \frac{\partial J_\eta}{\partial \eta} d\eta d\xi + \iint_{c,v} \frac{\partial J_\xi}{\partial \xi} d\eta d\xi = \iint_{c,v} (J_\xi S^{\Phi'} + D) d\eta d\xi$$

where $D = -\frac{\partial}{\partial \eta} \left(\frac{\Gamma_\Phi \xi}{J} q_2 \Phi_\xi \right) - \frac{\partial}{\partial \xi} \left(\frac{\Gamma_\Phi \xi}{J} q_2 \Phi_\eta \right)$

Therefore, $[(J_\eta)_e - (J_\eta)_w] \Delta \xi + [(J_\xi)_n - (J_\xi)_s] \Delta \eta = (J_\xi S^{\Phi'} + D)_P \Delta \eta \Delta \xi$ (1)

Let $\Phi = 1$, we can get the continuity equation

(now $S^{\Phi'}(\xi, \eta) = -\frac{\rho u r'_\eta}{J \xi}$)

$$F_e - F_w + F_n - F_s = (-\rho u r'_\eta)_P \Delta \eta \Delta \xi \quad (2)$$

In the above,

$$F_e = (\rho \xi \bar{u})_e \Delta \xi, \quad F_w = (\rho \xi \bar{u})_w \Delta \xi,$$

$$F_n = (\rho \xi \bar{v})_n \Delta \eta, \quad F_s = (\rho \xi \bar{v})_s \Delta \eta$$

Let $J_e = (J_\eta)_e \Delta \xi, \quad J_w = (J_\eta)_w \Delta \xi,$

$$J_n = (J_\xi)_n \Delta \eta, \quad J_s = (J_\xi)_s \Delta \eta,$$

by (1)-(2) $\times \Phi_P$, we get

$$(J_e - F_e \Phi_P) - (J_w - F_w \Phi_P) + (J_n - F_n \Phi_P) - (J_s - F_s \Phi_P) = (J_\xi S^{\Phi'} + D + \rho u r'_\eta \Phi)_P \Delta \eta \Delta \xi \quad (3)$$

By using the common discretization formula recommended in reference [6]

$$J - F \Phi_i = A(\Phi_i - \Phi_{i+1})$$

we can get

$$J_e - F_e \Phi_P = a_E(\Phi_P - \Phi_E), \quad J_w - F_w \Phi_P = a_W(\Phi_P - \Phi_W),$$

$$J_n - F_n \Phi_P = a_N(\Phi_P - \Phi_N), \quad J_s - F_s \Phi_P = a_S(\Phi_P - \Phi_S)$$

Let $b_P = (J_\xi S^{\Phi'} + D + \rho u r'_\eta \Phi)_P \Delta \eta \Delta \xi$, then equation (3) will change to

$$a_P \Phi_P = a_E \Phi_E + a_W \Phi_W + a_N \Phi_N + a_S \Phi_S + b_P \quad (4)$$

where

$$a_P = a_E + a_W + a_N + a_S,$$

$$a_E = D_e A \left(\frac{F_e}{D_e} \right) + [-F_e, 0],$$

$$a_W = D_w A \left(\frac{F_w}{D_w} \right) + [F_w, 0],$$

$$a_N = D_n A \left(\frac{F_n}{D_n} \right) + [-F_n, 0],$$

$$a_S = D_s A \left(\frac{F_s}{D_s} \right) + [F_s, 0],$$

D_e, D_w, D_n, D_s : diffusive coefficients on interfaces of the control volume

F_e, F_w, F_n, F_s : mass fluxes on interfaces of the control volume

The denotation $[|\omega_1, \omega_2|]$ indicates the larger between ω_1 and ω_2 .

In order to linearize source term b_P , let

$$(J_\xi S^{\Phi'} + D + \rho u r'_\eta \Phi)_P = S_C + S_P \Phi_P$$

By substituting this into equation (4) and making rearrangement, we get

$$a_P \Phi_P = a_E \Phi_E + a_W \Phi_W + a_N \Phi_N + a_S \Phi_S + b \quad (5)$$

Equation (5) is the discretized form of controlling equations on the computational plane, where

$$a_P = a_P' - S_P \Delta \eta \Delta \xi, \quad b = S_C \Delta \eta \Delta \xi$$

According to the different finite-difference approximating method of the convection terms,

function $A\left(\frac{F}{D}\right)$ has different expressions. Let

$$P = \frac{F}{D}, \text{ the expressions of function } A(|P|)$$

corresponding to the different finite-difference formats are listed in table 2.3.

Thus, we get the discretized forms of controlling differential equations on the computational plane.

Table 2.3 Function $A(|P|)$ Corresponding to the Different Difference Formats

Formats	$A(P)$
Central Difference	$1 - 0.5 P $
Upwind	1
HYBRID	$[0, 1 - 0.5 P]$
Power Law	$[0, (1 - 0.1 P)^3]$
Second-order Upwind	$A(P_e) = 1 + 0.5[-P_e, 0]$ $A(P_w) = 1 + 0.5[P_w, 0]$

2.4 The pressure correction equation and velocity correction formulae

We have got the discretized form of each controlling equation in the above section, but

we can not yet solve the flow field because the pressure remains unknown in the u and v momentum equations. These years, in solving this problem the SIMPLE (the semi-implicit couple of pressure and velocity) procedure proposed by S. V. Patanker etc [6] has found extensive application. The key of this procedure is to deduce the pressure correction equation and velocity correction formulae. At first, the pressure field is guessed to gain the corresponding velocity field. Generally, this velocity field does not satisfy the continuity equation. Therefore, the pressure correction equation is solved to get the correction pressure. Then the correction pressure and velocity correction formulae are used to modify the pressure and velocity fields, and this procedure is repeated until the convergence is attained.

Applying the SIMPLE procedure to the discretized common equation (4), we can obtain velocity correction formulae on the computational plane as follows.

$$\bar{u} = \bar{u}^* + r_\xi C^u p'_\eta \Delta \eta \Delta \xi \quad (6)$$

$$\bar{v} = \bar{v}^* + (B^v - r_\eta B^u) p'_\xi \Delta \eta \Delta \xi \quad (7)$$

While the pressure correction equation is

$$a_P p'_P = a_E p'_E + a_W p'_W + a_N p'_N + a_S p'_S + b \quad (8)$$

where

$$\begin{aligned} a_E &= (\rho \xi)_e L_{1e} \Delta \xi^2, \\ a_W &= (\rho \xi)_w L_{1w} \Delta \xi^2, \\ a_N &= (\rho \xi)_n L_{2n} \Delta \eta^2, \\ a_S &= (\rho \xi)_s L_{2s} \Delta \eta^2, \\ a_P &= a_E + a_W + a_N + a_S, \\ b &= -[(\rho \xi \bar{u}^*)_e \Delta \xi - (\rho \xi \bar{u}^*)_w \Delta \xi + (\rho \xi \bar{v}^*)_n \Delta \eta - \\ &\quad (\rho \xi \bar{v}^*)_s \Delta \eta] - (\rho r_\eta)_P \Delta \eta \Delta \xi u_P^* \\ L_1 &= -r_\xi C^u, \quad L_2 = -B^v + r_\eta B^u \end{aligned}$$

Let $p' = \Phi'$, we can get

$$a_P \Phi'_P = a_E \Phi'_E + a_W \Phi'_W + a_N \Phi'_N + a_S \Phi'_S + b \quad (9)$$

Thus we have obtained the pressure correction equation (8) or equation (9).

2.5 Some problems concerning the convergence and stability

For the convective terms, a finite-difference method of HYBRID combined with the second-order upwind format is used on the basis of the high convergence precision of HYBRID and the good stability of second-order

upwind. In the preliminary iterations HYBRID format is adopted, then the second-order upwind.

In order to advance the convergence rate, a strengthened SIMPLE procedure, i.e. the SIMPLEC procedure was put forth in reference [7]. The analysis in reference [7] showed that after adopting the SIMPLEC procedure, no under-relaxation would be needed for pressure, which meant that in the formula $p = p^* + \alpha_p p'$, α_p could be 1.0 to speed up convergence. The conclusion of reference [7] was aimed at the regular domain in the physical coordinates. In the transformation coordinates, the computation practice indicates that under-relaxation is still required for the pressure correction. Either for recirculation flow or for non-recirculation flow, it is generally appropriate to take $\alpha_p = 0.8$.

2.6 Boundary conditions and near-wall treatment

Currently, there are mainly two methods of turbulent treatment near the wall. The first method is to adopt a near-wall turbulent model: to lay very fine grids near the wall and solve the flow field from the rich turbulence area to the wall points, we can take $k_w = \varepsilon_w = 0$. The second method is to utilize the existing experimental results and experiential expressions, plus certain theoretical analysis, to give the changing rule of each parameter. This method is called the wall function method. Because of its saving computation time and its relative reliability, this method has found extensive application. This paper adopts the wall function method presented in reference [8].

The boundary condition of each equation is prescribed as follows.

$$\text{For } u \text{ equation, inlet given, outlet } \frac{\partial u}{\partial \eta} = 0,$$

$$\text{symmetrical boundary } \frac{\partial u}{\partial \xi} = 0, \text{ wall } u = 0. \text{ For } v$$

$$\text{equation, inlet given, outlet } \frac{\partial v}{\partial \eta} = 0, \text{ symmetrical}$$

$$\text{boundary } v = 0, \text{ wall } v = 0. \text{ For } w \text{ equation, inlet}$$

$$\text{given, outlet } \frac{\partial w}{\partial \eta} = 0, \text{ symmetrical boundary}$$

$w=0$, wall $w=0$. For k equation, inlet given to the following formulae: the main jet $k=C_k U_{im}^2$, the annular jet $k=C_k U_{om}^2$ (according to the inlet turbulence quantity, we can take $C_k=0.001-0.06$), outlet $\frac{\partial k}{\partial \eta} = 0$, symmetrical

boundary $\frac{\partial k}{\partial \xi} = 0$, wall $\frac{\partial k}{\partial \xi} = 0$. For ε equation,

inlet given to the following formulae: the main jet $\varepsilon = k^{\frac{3}{2}} / (0.005 R_{in})$, the annular jet $\varepsilon = k^{\frac{3}{2}} / [0.005 (R_1 - R_{in})]$, outlet $\frac{\partial \varepsilon}{\partial \eta} = 0$,

symmetrical boundary $\frac{\partial \varepsilon}{\partial \xi} = 0$, wall $\frac{\partial \varepsilon}{\partial \xi} = 0$. For

p' equation, on all boundaries $\frac{\partial p'}{\partial n} = 0$. (n is the normal of that boundary.)

3 Comparison analysis of computational results with experimental data

A numerical prediction has been made with the experimental conditions of confined coaxial jets with imposed pressure gradient. The inlet axial velocity u is given the real values probed in the experiment. As the velocity on each point of the nozzle exit plane is axial, the radial velocity of the confinement inlet $v=0$. Because of non-swirling, on each point of the confinement inlet $w=0$. According to the experimental conditions and real measuring results, the flow on the nozzle exit plane is dominated by the molecular viscous force. Therefore, the inlet turbulent kinetic energy and its diffusive rate are all approximately zero, and the k and ε values are prescribed as $k=0$, $\varepsilon=0$. The inner nozzle lip is so thin that its thickness can be taken as zero. In accordance with the inlet conditions as well as the geometrical configuration of the confinement, computation has been made using the calculating code of this paper. The comparison of the computation and experimentation results is shown in Fig. 3.1 and Fig. 3.2. In each figure, the continuous curve indicates the computation and the scattered points indicate the experimentation results. Fig.

3.1 shows the wall static pressure. The abscissa 'X/D' indicates the normalized value of the axial distance with the confinement inlet diameter serving as the normalizing unit. The ordinate 'P' indicates the normalized pressure $(p_w - p_j) / (\frac{1}{2} \rho u_j^2)$

(p_w is wall static pressure, p_j and u_j are static pressure and axial velocity at the symmetrical axis point of the nozzle outlet plane). There is rather fine agreement of the computation results with the experimentation results. The difference is that the computation curve lags slightly behind the experimental data points.

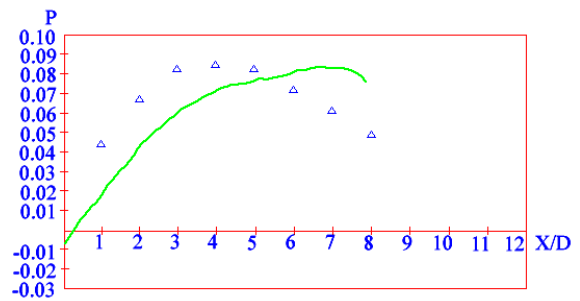


Fig. 3.1 Wall Static Pressure

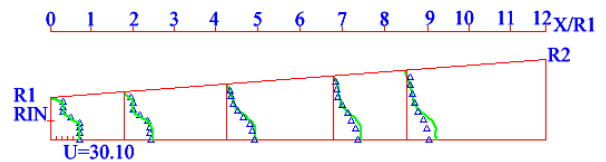


Fig. 3.2 Profile of Axial Velocity

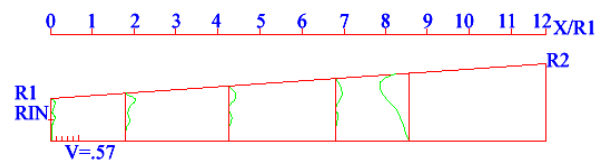


Fig. 3.3 Profile of Radial Velocity

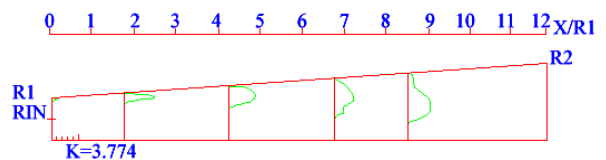


Fig. 3.4 Profile of Turbulent Kinetic Energy

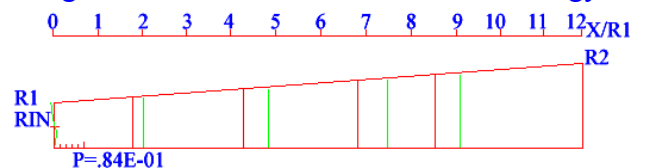


Fig. 3.5 Profile of Static Pressure

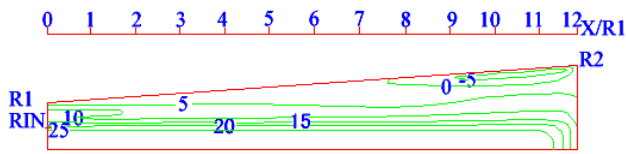


Fig. 3.6 Contours of Axial Velocity

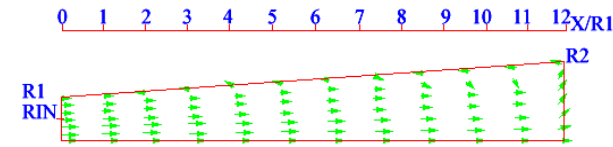


Fig. 3.7 Velocity Vector Profile on the Meridian Plane

4 The numerical prediction of a contra-swirling jet with imposed pressure gradient

A numerical prediction of a contra-swirling jet with imposed pressure gradient has been made, with the geometrical configuration of inlet radius $R_1=0.25m$, outlet radius $R_2=0.35m$, confinement length $L=1.5m$ and inner nozzle radius $R_{in}=0.1m$. Axial velocities of the inner and annular nozzles are given uniform profiles, with the inner nozzle $u_i=30m/s$ and the annular nozzle $u_o=20m/s$. The inlet velocities on the meridian plane are axial, so the radial velocity $v=0$. Circumferential velocities are given by the following formulae: the main jet $w=3.6u(r/R_{in})$, the annular jet $w=-3.6u[r/(R-R_{in})]$. The inlet turbulent kinetic energy k and its diffusive rate ϵ are still given the same as in section 1.6, with $C_k=0.03$. According to the above inlet condition, computation has been made using the calculating code of this paper. The results are shown in Fig. 4.1-4.7.

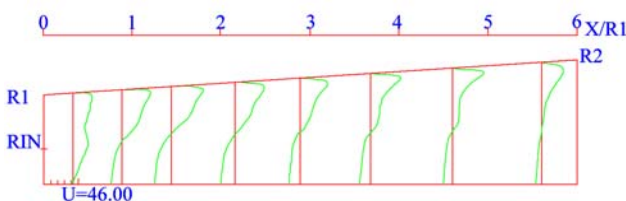


Fig. 4.1 Profile of Axial Velocity

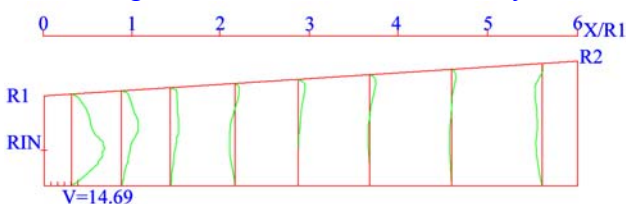


Fig. 4.2 Profile of Radial Velocity

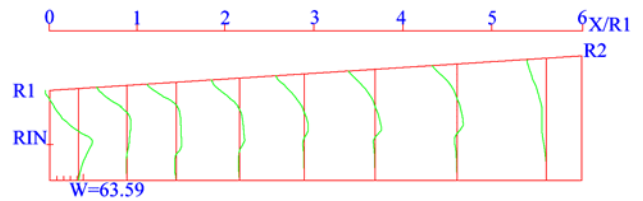


Fig. 4.3 Profile of Circumferential Velocity

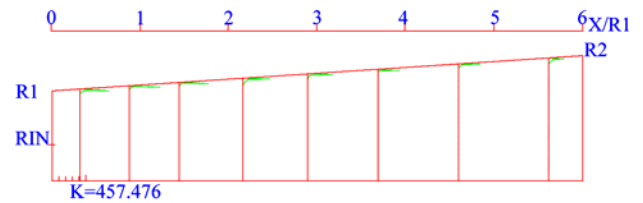


Fig. 4.4 Profile of Turbulent Kinetic Energy

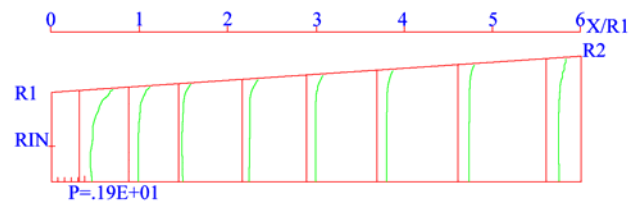


Fig. 4.5 Profile of Static Pressure

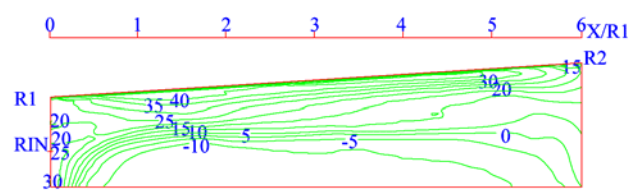


Fig. 4.6 Contours of Axial Velocity

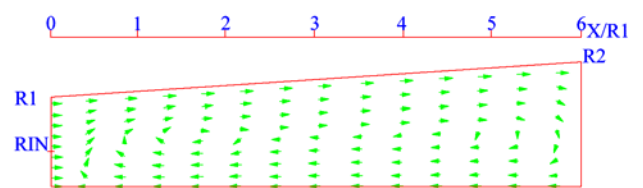


Fig. 4.7 Velocity Vector Profile on the Meridian Plane

5 The numerical prediction of a contra-swirling jet with sudden expanding confinement of constant section

A numerical prediction of a contra-swirling jet with sudden expanding confinement of constant section has been made, with the geometrical configuration of inlet radius $R_1=0.1m$, inner nozzle radius $R_{in}=0.0195m$, duct radius $R_2=0.2m$ and confinement length $L=1.5m$. Inlet axial and circumferential velocity profiles

have been given, with the inlet axial velocity profile shown in Fig. 5.1 and the circumferential in Fig. 5.3. The inlet velocities on the meridian plane are axial, so the radial velocity $v=0$. The inlet turbulent kinetic energy k and its diffusive rate ε are still given the same as in section 1.6, with $C_k=0.03$. According to the above inlet condition, computation has been made using the calculating code of this paper. The results are shown in Fig. 5.1-5.7.

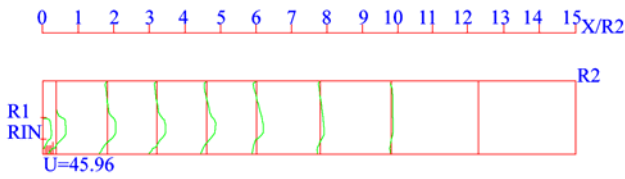


Fig. 5.1 Profile of Axial Velocity

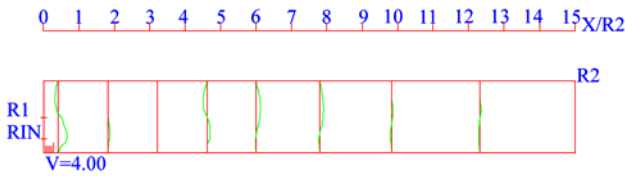


Fig. 5.2 Profile of Radial Velocity

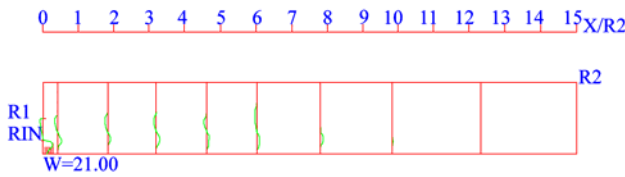


Fig. 5.3 Profile of Circumferential Velocity

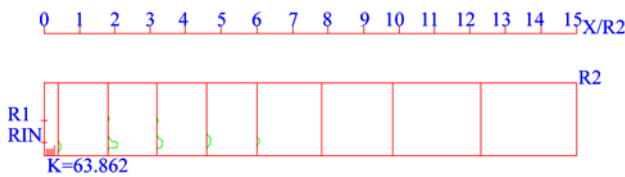


Fig. 5.4 Profile of Turbulent Kinetic Energy

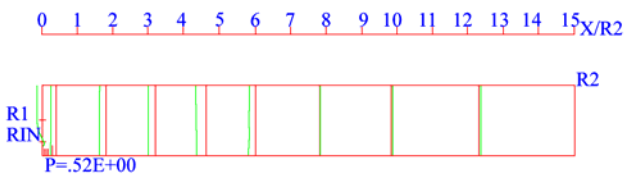


Fig. 5.5 Profile of Static Pressure

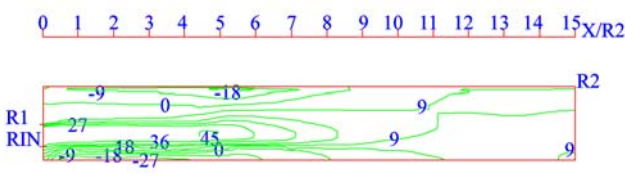


Fig. 5.6 Contours of Axial Velocity

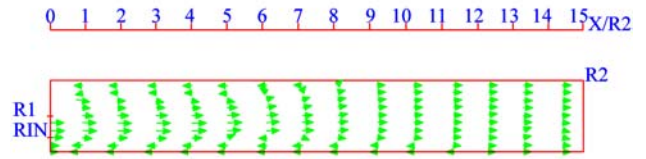


Fig. 5.7 Velocity Vector Profile
on the Meridian Plane

6 Conclusions

1) In this paper, by applying the non-orthogonal coordinate transformation procedure in the Cartesian coordinate system put forth in reference [1] to the meridian plane in the cylindrical coordinate system, any axis-symmetrical domain could be transformed from being irregular into regular. The other characteristic of this paper is that the velocity component solved on the computational plane is the very velocity on the original physical plane.

2) A numerical prediction has been made by applying the procedure of this paper to the experimental data presented in reference [2] for a non-swirling coaxial confined jet with imposed adverse pressure gradient. The comparison of the computation results with the experimentation results shows a rather fine agreement. It shows the calculation procedure of this paper is practicable. Of course, for the prediction precision of the swirling case, further experimental verification is still required.

3) The computation shows that it is difficult to make numerical predictions of coaxial confined swirling (especially contra-swirling) jets with sudden expanding confinement. There is a rather narrow convergence limit to the relaxation factor.

4) The computation shows that the magnitude and profile of inlet turbulent parameters have remarkable influence upon the precision of numerical predictions. Therefore, realistic inlet turbulent parameters must be specified if quantitatively correct results are desired.

Appendix Γ_Φ and S^Φ expressions on the computational plane

$$\Phi = v:$$

$$\Gamma_\Phi = \mu_{eff}$$

$$S^{\Phi'} = S^{v'} = -\frac{1}{J} \frac{\partial p}{\partial \xi} - 2\mu_{eff} \frac{v}{w_r^2(\eta)\xi^2} + \frac{\rho w^2}{w_r(\eta)\xi} - \frac{r_\eta}{J} \frac{\partial}{\partial \xi} \left(\mu_{eff} \frac{1}{J} \frac{\partial u}{\partial \xi} \right) + \frac{\partial}{\partial \eta} \left(\mu_{eff} \frac{1}{J} \frac{\partial u}{\partial \xi} \right) + \frac{1}{J \xi} \frac{\partial}{\partial \xi} \left(\zeta \mu_{eff} \frac{1}{J} \frac{\partial v}{\partial \xi} \right) - \frac{\rho u v r_\eta}{J \xi} + \frac{\mu_{eff}}{J^2 \xi} \left(r_\zeta \frac{\partial v}{\partial \eta} - r_\eta \frac{\partial v}{\partial \xi} \right)$$

$\Phi = u:$

$$\Gamma_\Phi = \mu_{eff}$$

$$S^{\Phi'} = S^{u'} = -\left(\frac{\partial p}{\partial \eta} - \frac{r_\eta}{J} \frac{\partial p}{\partial \xi} \right) - \frac{r_\eta}{J} \frac{\partial}{\partial \xi} \left[\mu_{eff} \left(\frac{\partial u}{\partial \eta} - \frac{r_\eta}{J} \frac{\partial u}{\partial \xi} \right) \right] + \frac{\partial}{\partial \eta} \left[\mu_{eff} \left(\frac{\partial u}{\partial \eta} - \frac{r_\eta}{J} \frac{\partial u}{\partial \xi} \right) \right] + \frac{1}{J \xi} \frac{\partial}{\partial \xi} \left[\zeta \mu_{eff} \left(\frac{\partial v}{\partial \eta} - \frac{r_\eta}{J} \frac{\partial v}{\partial \xi} \right) \right] - \frac{\rho u v r_\eta}{J \xi} + \frac{\mu_{eff}}{J^2 \xi} \left(r_\zeta \frac{\partial u}{\partial \eta} - r_\eta \frac{\partial u}{\partial \xi} \right)$$

$\Phi = w:$

$$\Gamma_\Phi = \mu_{eff}$$

$$S^{\Phi'} = S^{w'} = -\frac{\rho v w}{w_r(\eta)\xi} + \frac{1}{w_r(\eta)\xi} \left(\mu_{eff} \frac{1}{J} \frac{\partial w}{\partial \xi} \right) - \frac{1}{J} \frac{\partial}{\partial \xi} \left(\mu_{eff} \frac{w}{w_r(\eta)\xi} \right) - \frac{2}{w_r(\eta)\xi} \left(\mu_{eff} \frac{w}{w_r(\eta)\xi} \right) - \frac{\rho u w r_\eta}{J \xi} + \frac{\mu_{eff}}{J^2 \xi} \left(r_\zeta \frac{\partial w}{\partial \eta} - r_\eta \frac{\partial w}{\partial \xi} \right)$$

$\Phi = k:$

$$\Gamma_\Phi = \frac{\mu_{eff}}{\sigma_k}$$

$$S^{\Phi'} = S^{k'} = G - \rho \varepsilon - \frac{\rho u k r_\eta}{J \xi} + \frac{\mu_{eff}}{J^2 \xi} \frac{\partial k}{\sigma_k} \left(r_\zeta \frac{\partial k}{\partial \eta} - r_\eta \frac{\partial k}{\partial \xi} \right)$$

$\Phi = \varepsilon:$

$$\Gamma_\Phi = \frac{\mu_{eff}}{\sigma_\varepsilon}$$

$$S^{\Phi'} = S^{\varepsilon'} = \frac{\varepsilon}{k} (C_1 G - C_2 \rho \varepsilon) - \frac{\rho u \varepsilon r_\eta}{J \xi} + \frac{\mu_{eff}}{J^2 \xi} \frac{\partial \varepsilon}{\sigma_\varepsilon} \left(r_\zeta \frac{\partial \varepsilon}{\partial \eta} - r_\eta \frac{\partial \varepsilon}{\partial \xi} \right)$$

In both cases ($\Phi = k$ and $\Phi = \varepsilon$):

$$G = \mu_{eff} \left\{ 2 \left[\left(\frac{\partial u}{\partial \eta} - \frac{r_\eta}{J} \frac{\partial u}{\partial \xi} \right)^2 + \left(\frac{1}{J} \frac{\partial v}{\partial \xi} \right)^2 + \left(\frac{v}{w_r(\eta)\xi} \right)^2 \right] + \left(\frac{1}{J} \frac{\partial u}{\partial \xi} + \frac{\partial v}{\partial \eta} - \frac{r_\eta}{J} \frac{\partial v}{\partial \xi} \right)^2 + \left[\left(\frac{\partial w}{\partial \eta} - \frac{r_\eta}{J} \frac{\partial w}{\partial \xi} \right)^2 + \left(\frac{1}{J} \frac{\partial w}{\partial \xi} - \frac{w}{w_r(\eta)\xi} \right)^2 \right] \right\}$$

[1] M Faghri, E M Sparrow and A T Prata. Finite-difference solutions of convection-diffusion problems in irregular domains, using a non-orthogonal coordinate transformation. *Numerical Heat Transfer*, Vol. 7, pp 183-209, 1984.

[2] D W Choi, F B Gessner and G C Oates. Measurements of confined, coaxial jet mixing with pressure gradient. *Journal of Fluids Engineering*, Vol. 108, pp 39-46, 1986.

[3] J F Thompson, F C Thames and C W Mastin. Automatic numerical generation of body-fitted curvilinear coordinate system for field containing any number of arbitrary two-dimensional bodies. *Journal of computational physics*, Vol. 15, pp 299-319, 1974.

[4] J F Thompson, Z U A Warsi and C W Mastin. Boundary-fitted coordinate systems for numerical solution of partial differential equations, a review. *Journal of computational physics*, Vol. 47, pp.1-108, 1982.

[5] M T Abujelala and D G Lilley. Limitations and empirical extensions of the k-ε model as applied to turbulent confined swirling flows. *AIAA Aerospace Sciences Meeting, 22nd*, Reno, NV, AIAA paper 84-0441, pp 1-10, Jan. 9-12, 1984.

[6] S V Patanker. *Numerical heat transfer and fluid flow*. Hemisphere Publishing Corp., 1981.

[7] J P Van Doormaal, G D Raithby. Enhancement of the SIMPLE method for predicting incompressible fluid flows. *Numerical Heat Transfer*, Vol. 7, pp 147-163, 1984.

[8] G Comini and S Del Giudice. A k-ε model of turbulent flow. *Numerical Heat Transfer*, Vol. 8, pp 133-147, 1985.

References